PERGAMON

International Journal of Heat and Mass Transfer 42 (1999) 1037–1045

International Journal of HEAT and MASS TRANSFER

Thermoconvective instability in a rotating magnetic field

M. P. Volz*, K. Mazuruk

Space Science Laboratory, NASA Marshall Space Flight Center, Huntsville, AL 35812, U.S.A.

Received 6 June 1997; in final form 2 May 1998

Abstract

The effect of a rotating magnetic field (RMF) on the stability of a fluid contained in a cylindrical column and heated from below is investigated. The RMF increases the critical Rayleigh number for asymmetric flow modes but does not affect the onset of instability for axisymmetric modes. The critical Rayleigh number is dependent upon the relative penetration of the magnetic field into the cylinder and the Prandtl number of the fluid. Instability first develops in the form of a single asymmetric meridional roll rotating around the axis of the cylinder, driven by the azimuthal component of the magnetic field.

Nomenclature

$A_{n,m}$ coefficients in velocity field representation
b time and angular independent magnetic field component
B magnetic field
$C_{n,m}$ coefficients in temperature field representation
D $\mathrm{ber}_0^2(K)+\mathrm{bei}_0^2(K)$
F Lorentz force
g acceleration of gravity
Ha Hartmann number
j electric current density
k continuous modal index
K skin depth parameter, r_0/δ
L operator, $(\partial/\partial r)(1/r)(\partial/\partial r)r$
L_m operator, $(\partial^2/\partial r^2)+(1/r)(\partial/\partial r)-(m^2/r)$
m, n discrete modal indices
M matrix
P Prandtl number
P_0 pressure
$q_{n,m}$ normalization coefficients
r radial coordinate
$\hat{\mathbf{r}}$ unit radial vector
Ra Rayleigh number
Ra^c critical Rayleigh number
Rm magnetic Reynolds number
t time
T temperature
T_c constant reference temperature
Tm magnetic Taylor number
Tm^c critical magnetic Taylor number
$\mathbf{v}$ fluid velocity
V perturbation fluid velocity
z axial coordinate
$\hat{\mathbf{z}}$ unit axial vector.

Greek symbols

α coefficient of thermal expansion
β temperature gradient
$\beta_{n,m}$ eigenvalues
δ skin depth
σ_{nN} delta function
κ thermal diffusivity
μ_0 permeability of free space
ν kinematic viscosity
ρ density
σ electrical conductivity
φ azimuthal coordinate
$\hat{\boldsymbol{\varphi}}$ unit azimuthal vector
ω angular frequency of magnetic field
$\bar{\omega}$ characteristic fluid rotation frequency
Ω angular velocity of fluid, v_φ/r.

Subscripts

r radial component
z axial component
φ azimuthal component
0 reference level.

* Corresponding author

0017–9310/98 $19.00
PII: S0017–9310(98)00168–9

1. Introduction

The application of an RMF has proven to be quite beneficial for a number of solidification processes. In particular, single crystal growth experiments have demonstrated an improvement in the grown material when an RMF was applied [1–3]. An RMF can reduce sedimentation, enhance the stirring of multicomponent liquids, and increase thermal symmetry at the solidification front. These benefits are closely linked to the flow patterns that an RMF induces. As a result, there have been several theoretical [4–8] and experimental [9–13] investigations on the fluid flow generated by an RMF. These investigations have examined laminar flow, turbulence and the criterion for the onset of Reynolds instability. In this paper we investigate the onset of Rayleigh–Benard convection in a vertical cylinder when an RMF is applied. Such a convection can play a significant role in a number of crystal growth processes and can introduce inhomogeneities and other deleterious effects in the grown crystals. Thus, an understanding of the effect that an RMF has on thermoconvective instability can be quite important.

The problem of thermoconvective stability in a cylinder, both with and without cylinder rotation, has been previously addressed [14–16]. The effect of an RMF on thermoconvective stability in a cylinder is somewhat analogous to that of cylinder rotation. Whereas for cylinder rotation the critical Rayleigh number is determined as a function of the Taylor number, for the application of an RMF the critical Rayleigh number is determined as a function of the magnetic Taylor number. The application of an RMF also involves a second independent variable which is the relative penetration of the magnetic field into the fluid, as characterized by the skin depth. However, the application of an RMF results in a flow pattern significantly different than that obtained by cylinder rotation. This is a result of the different boundary conditions at the cylinder wall. For cylinder rotation, the angular velocity of the fluid at the wall is equal to the applied angular velocity of the cylinder. When an RMF is applied, the angular velocity of the fluid is zero at the cylinder wall. The flow generated by an RMF is similar to cylinder rotation in yet another respect. For two concentric cylinders of similar radii, there will be a critical value of the Taylor number where instabilities occur. When an RMF is applied, there will be a critical value of the magnetic Taylor number where instabilities of the Taylor vortex-type might also be expected. This paper is concerned with flow below this critical value, where Stokes flow or weakly non-linear flow exists.

This paper first presents the magnetic field, electromagnetic force, and fluid flow generated by an RMF in an isothermal vertical cylinder [5]. The dependence of the electromagnetic force and fluid flow on the skin depth is examined. The onset of steady thermal convection is then calculated, using linear stability analysis and the Boussinesq approximation. The solutions to this problem are based on expansions of eigenfunctions which are themselves solutions to the thermoconvective stability problem without an RMF applied. The nature of the convection and temperature distributions at the onset of convection are described. Finally, the limitations of the calculations and the circumstances of their applicability are discussed.

2. Electromagnetic field equations

We consider an incompressible liquid metal of electrical conductivity σ inside a cylinder of infinite vertical extent and radius r_0. A rotating magnetic field with an induction B_0 and angular frequency ω is applied to the fluid. It is convenient to work with complex numbers, with the real parts corresponding to the physical quantities. As $r \to \infty$, the imposed magnetic field can be written as

$$\mathbf{B}_{r\to\infty} = (\hat{\mathbf{r}} - i\hat{\boldsymbol{\varphi}})B_0\, \mathrm{e}^{i(\omega t-\varphi)} \tag{1}$$

where t is time and $\hat{\mathbf{r}}$ and $\hat{\boldsymbol{\varphi}}$ are unit vectors in the cylindrical coordinate system. The cylindrical coordinates (r, φ, z) used to describe the system and the imposed external magnetic field are shown in Fig. 1. The magnetic field and resulting fluid flow are confined to the (r, φ) plane.

The advection–diffusion equation describing the magnetic field distribution inside the cylinder is

$$\frac{\partial \mathbf{B}}{\partial t} = \nabla \times (\mathbf{v} \times \mathbf{B}) + \frac{1}{\mu_0 \sigma}\nabla^2 \mathbf{B} \tag{2}$$

where $\mathbf{v}$ is the fluid velocity and μ_0 is the permeability of free space. The ratio of the convective to diffusive terms scales as the magnetic Reynolds number

$$Rm = \mu_0 \sigma r_0 v. \tag{3}$$

When Rm is small compared to unity, the $\mathbf{v} \times \mathbf{B}$ term can be neglected. This is the case for most practical laboratory

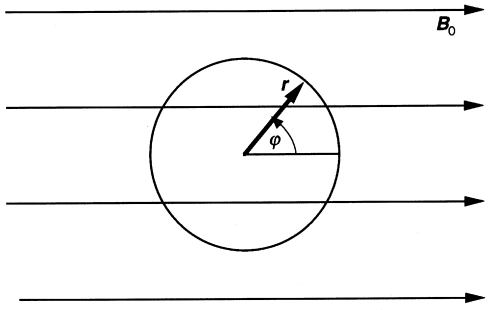

Fig. 1. Schematic of the physical system. The cylinder is filled with liquid metal and the applied external magnetic field B_0 rotates with angular frequency ω in the φ-direction.

applications and corresponds to the situation where the influence of the fluid flow on the magnetic field can be neglected. This so-called 'solid body approximation' will be adopted here. We seek a solution of the form

$$\mathbf{B} = B_r\hat{\mathbf{r}} + B_\varphi\hat{\boldsymbol{\varphi}} \tag{4}$$

where

$$B_r = b_r(r)\,\mathrm{e}^{i(\omega t-\varphi)}, \quad B_\varphi = b_\varphi(r)\,\mathrm{e}^{i(\omega t-\varphi)}. \tag{5}$$

The solution must satisfy equation (1) and **B** must be continuous at r_0. Also, from the symmetry of the problem,

$$\frac{\partial \mathbf{B}}{\partial z} = B_z = 0. \tag{6}$$

The total magnetic field can then be calculated from the following equations:

$$\nabla^2\mathbf{B} = \frac{i}{\delta^2}\mathbf{B}, \quad \nabla\cdot\mathbf{B} = 0, \quad \text{for } r \leqslant r_0 \tag{7}$$

$$\nabla\times\mathbf{B} = 0, \quad \nabla\cdot\mathbf{B} = 0, \quad \text{for } r > r_0 \tag{8}$$

where the skin depth $\delta = (\sigma\omega\mu_0)^{-1/2}$. The solution for the magnetic field distribution inside the cylinder is

$$b_r = \frac{2B_0\delta}{r\,\mathrm{e}^{3\pi i/4}}\frac{J_1\left(\frac{r}{\delta}\mathrm{e}^{3\pi i/4}\right)}{J_0(K\,\mathrm{e}^{3\pi i/4})} = \frac{2B_0\delta}{r\,\mathrm{e}^{3\pi i/4}}\frac{\mathrm{ber}_1(r/\delta)+i\,\mathrm{bei}_1(r/\delta)}{\mathrm{ber}_0(K)+i\,\mathrm{bei}_0(K)} \tag{9}$$

$$b_\varphi = -i\frac{\partial}{\partial r}(rb_r) = -2iB_0\left((\mathrm{ber}_0(r/\delta)+i\,\mathrm{bei}_0(r/\delta)) - \mathrm{e}^{\frac{-3\pi i}{4}}\frac{\delta}{r}(\mathrm{ber}_1(r/\delta)+i\,\mathrm{bei}_1(r/\delta))\right)\Big/\left(\mathrm{ber}_0(K)+i\,\mathrm{bei}_0(K)\right). \tag{10}$$

Outside the cylinder

$$b_r = B_0 - \frac{B_0 r_0^2}{r^2}\left(1-\frac{2(\mathrm{ber}_1(K)+i\,\mathrm{bei}_1(K))}{\mathrm{e}^{3\pi i/4}K(\mathrm{ber}_0(K)+i\,\mathrm{bei}_0(K))}\right) \tag{11}$$

$$b_\varphi = -iB_0 + \frac{iB_0 r_0^2}{r^2}\left(1-\frac{2(\mathrm{ber}_1(K)+i\,\mathrm{bei}_1(K))}{\mathrm{e}^{3\pi i/4}K(\mathrm{ber}_0(K)+i\,\mathrm{bei}_0(K))}\right) \tag{12}$$

where $K = r_0/\delta$ is the dimensionless skin depth parameter and J_0 and J_1 are Bessel functions. The real and imaginary parts of $J_n(x\,\mathrm{e}^{3\pi i/4})$ are denoted by $\mathrm{ber}_n(x)$ and $\mathrm{bei}_n(x)$.

The induced electric current density is calculated from the equation

$$\mathbf{j} = \frac{1}{\mu_0}\nabla\times\mathbf{B}. \tag{13}$$

The only non-vanishing component is

$$j_z = \frac{-2B_0\,\mathrm{e}^{\pi i/4}}{\mu_0\delta}\left(\frac{\mathrm{ber}_1(r/\delta)+i\,\mathrm{bei}_1(r/\delta)}{\mathrm{ber}_0(K)+i\,\mathrm{bei}_0(K)}\right)\mathrm{e}^{i(\omega t-\varphi)}. \tag{14}$$

The two non-vanishing components of the Lorentz force are obtained from the following formulas:

$$F_r = -Re(j_z)\,Re(B_\varphi), \quad F_\varphi = Re(j_z)\,Re(B_r). \tag{15}$$

These equations result in both a time-independent component of force and an oscillatory component of frequency 2ω. The oscillatory component of the force induces, in general, an oscillatory motion of the fluid. However, the inertia of the fluid will not allow it to follow the relatively high frequency oscillating force component and the amplitude of the oscillating flow will be negligible [17]. The time averaged value of this oscillating force component can also be non-zero due to the presence of the nonlinear advection term in the Navier–Stokes equations. However, for purely azimuthal flow, this advection term is zero, and therefore the oscillating force will not generate any stationary flow components. The r-component of force is compensated by a change in the pressure and does not affect the fluid motion. Thus, the only force which drives fluid motion is the time-independent φ-component

$$F_\varphi = \frac{2B_0^2}{\mu_0 r}\left(\frac{\mathrm{ber}_1^2(r/\delta)+\mathrm{bei}_1^2(r/\delta)}{\mathrm{ber}_0^2(K)+\mathrm{bei}_0^2(K)}\right). \tag{16}$$

The dependence of F_φ on r for three different values of K is shown in Fig. 2. F_φ is normalized by

$$F_0 = \frac{2B_0^2}{\mu_0 r_0}. \tag{17}$$

For small values of K, F_φ is a linear function of r. As K increases, the force is confined more and more to near the cylinder wall. It should also be noted that for each value of $r < r_0$, there is a finite value of K for which F_φ reaches a maximum.

3. Azimuthal fluid flow

The azimuthal velocity is independent of both φ and t. The Navier–Stokes equation can be written:

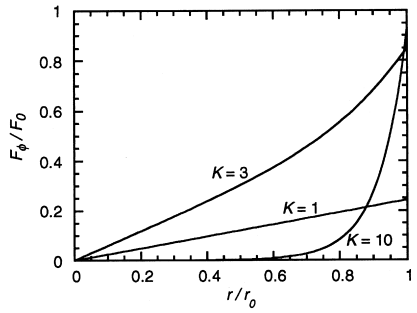

Fig. 2. Azimuthal Lorentz force vs. r.

$$Lv_\varphi = -\frac{F_\varphi}{v\rho}, \tag{18}$$

where v is the kinematic viscosity, ρ is the density, and

$$L = \frac{\partial}{\partial r}\frac{1}{r}\frac{\partial}{\partial r}r. \tag{19}$$

The solution to equation (18) can be written

$$v_\varphi = \frac{v_0 K^2 r}{r_0 D}\sum_{n=0}^{\infty}\frac{(1-(r/r_0)^{4n+2})(K/2)^{4n}}{(2n+1)(n+1)!(n+1)!(2n+1)!} \tag{20}$$

where

$$v_0 = \frac{B_0^2 r_0}{16\mu_0 v\rho} \tag{21}$$

and $D = \mathrm{ber}_0^2(K)+\mathrm{bei}_0^2(K)$. In the low frequency approximation, only the leading term of the series expansion needs to be kept:

$$v_\varphi = \frac{B_0^2\omega\sigma}{16v\rho}r(r_0^2-r^2). \tag{22}$$

In the high frequency approximation, when $K \gg 1$,

$$v_\varphi = \frac{B_0^2}{K^2 v\rho\mu_0}\left(r - r_0 \mathrm{e}^{-\sqrt{2}K\left(1-\frac{r}{r_0}\right)}\right). \tag{23}$$

Both the magnitude and frequency of the applied magnetic field can be modified to affect the fluid flow. These properties of the magnetic field have been separated in equation (20) with $v_0 \propto B_0^2$ and $K \propto \omega^{-1/2}$. By keeping v constant, the dependence of v_φ on K can be determined. This is shown in Fig. 3, where $v_\varphi^{\max}$ is plotted as function of K. The maximum value of v_φ occurs at different values of r, depending on K. For a fixed magnetic field strength, the maximum fluid rotation is obtained when $K = 2.35$. The dependence of v_φ on r is shown in Fig. 4. For K much less than 1, $v_\varphi/v_\varphi^{\max}$ is essentially independent of K. As K becomes larger, $v_\varphi^{\max}$ occurs at increasingly larger values of r.

4. Thermoconvective stability analysis

We now consider the onset of natural convection in the fluid when a negative temperature gradient is applied.

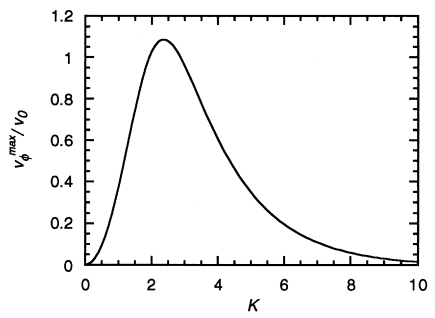

Fig. 3. Maximum azimuthal fluid velocity vs. K.

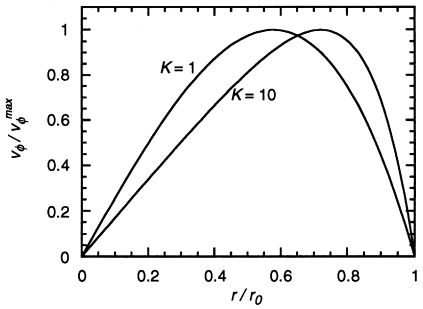

Fig. 4. Azimuthal fluid velocity vs. r for $K = 1$ and $K = 10$.

The initial velocity, temperature, pressure, and density distributions are

$$v_r = v_z = 0, \quad v_\varphi \tag{24}$$

$$T_0 = T_c - \beta z \tag{25}$$

$$\nabla P_0 = -\rho_0(1+\alpha\beta z)g\hat{\mathbf{z}} + F_r\hat{\mathbf{r}} \tag{26}$$

$$\rho = \rho_0(1+\alpha\beta z) \tag{27}$$

where v_φ is the azimuthal velocity resulting from the application of a rotating magnetic field and is defined in equation (20), T_c is a reference temperature, β is the negative temperature gradient, α is the coefficient of thermal expansion, g is the acceleration of gravity, and F_r is defined in equation (15). The initial velocity, temperature, and pressure are perturbed by V'. T', and P', and substituted into the Navier–Stokes and heat transfer equations. Neglecting products of perturbation terms, the z-component of the Navier–Stokes perturbation equation and the heat transfer equation become

$$\frac{\partial V_z'}{\partial t} + \frac{v_\varphi}{r}\frac{\partial V_z'}{\partial \varphi} = g\alpha T' + v\nabla^2 V_z' \tag{28}$$

$$\frac{\partial T'}{\partial t} + \frac{v_\varphi}{r}\frac{\partial T'}{\partial \varphi} = \beta V_z' + \kappa\nabla^2 T' \tag{29}$$

where κ is the thermal diffusivity. The r- and φ-components of the perturbed velocity do not couple to the perturbed temperature and need not be considered further.

The stationary spectral modes which are solutions to this problem can be written in the form

$$V_z'(r,\varphi,z) = V_{n,m,k}'(r)\,\mathrm{e}^{im(\bar{\omega}t-\varphi)}\,\mathrm{e}^{ikz} + cc \tag{30}$$

$$T'(r,\varphi,z) = T_{n,m,k}'(r)\,\mathrm{e}^{im(\bar{\omega}t-\varphi)}\,\mathrm{e}^{ikz} + cc \tag{31}$$

where n and m are discrete modal indices, k is a continuous index, and $\bar{\omega}$ is a characteristic rotational frequency which yet needs to be determined. It has been proven mathematically by Proctor [18] that the case of $k = 0$ corresponds to the lowest eigenvalue for a given set of indices (n, m). We therefore set $k = 0$.

Given the form of the solutions in equations (30) and (31), equations (28) and (29) can be written

$$(L_m + im(\Omega - \bar{\omega}))V = -RaT \tag{32}$$

$$(L_m + imP(\Omega - \bar{\omega}))T = -V \tag{33}$$

where

$$L_m = \frac{\partial^2}{\partial r^2} + \frac{1}{r}\frac{\partial}{\partial r} - \frac{m^2}{r} \tag{34}$$

$\Omega = v_\varphi/r$, P is the Prandtl number, Ra is the Rayleigh number with r_0 used as the length scale, V is the perturbed velocity in the z-direction, T is the perturbed temperature, and both V and T are functions of r only. The above equations are non-dimensionalized by scaling the length, frequency, velocity, pressure, and temperature with r_0, v/r_0^2, v/r_0, $\rho v^2/r_0^2$, and $\beta r_0 v/\kappa$, respectively. Equations (32) and (33) are solved for the case of adiabatic sidewalls with boundary conditions

$$V = T = 0, \quad \text{at } r = 0 \tag{35}$$

$$V = \frac{\partial T}{\partial r} = 0, \quad \text{at } r = 1. \tag{36}$$

We first develop a series of functions $V_{n,m}$ and $T_{n,m}$ upon which the solution of V and T will be expanded. The functions are solutions of the following simplified system:

$$L_m V_{n,m} = -\beta_{n,m}^2 T_{n,m} \tag{37}$$

$$L_m T_{n,m} = -\beta_{n,m}^2 V_{n,m} \tag{38}$$

where $\beta_{n,m}$ are eigenvalues to be determined. These equations describe the thermoconvective problem in a vertical cylinder when no RMF is applied. The boundary conditions (35)–(36) imposed on V and T are also imposed on $V_{n,m}$ and $T_{n,m}$, respectively. The solutions of this eigenvalue problem are

$$V_{n,m} = \frac{1}{\sqrt{q_{n,m}}}[I_m(\beta_{n,m})J_m(\beta_{n,m}r) - J_m(\beta_{n,m})I_m(\beta_{n,m}r)] \tag{39}$$

$$T_{n,m} = \frac{1}{\sqrt{q_{n,m}}}[I_m(\beta_{n,m})J_m(\beta_{n,m}r) + J_m(\beta_{n,m})I_m(\beta_{n,m}r)] \tag{40}$$

where I_m is a modified Bessel function

$$q_{n,m} = J_m^2(\beta_{n,m})I_{m-1}(\beta_{n,m})I_{m+1}(\beta_{n,m}) \tag{41}$$

and $q_{n,m}$ are normalization coefficients such that the above system of eigenfunctions is orthonormal in the following sense:

$$\int_0^1 V_{n,m}(r)T_{N,m}(r)r\,\mathrm{d}r = \delta_{nN}. \tag{42}$$

The eigenvalues $\beta_{n,m}$ are solutions of the following equation:

$$\frac{\partial}{\partial \beta}[I_m(\beta)J_m(\beta)] = 0. \tag{43}$$

The solutions of V and T can be expanded into the above set of functions:

$$V = \sum_n A_{n,m}V_{n,m}, \quad T = \sum_n C_{n,m}T_{n,m} \tag{44}$$

where $A_{n,m}$ and $C_{n,m}$ are complex coefficients which need to be determined. Using the orthonormality condition, the following system of matrix equations are obtained:

$$RaC_{N,m} = \beta_{N,m}^2 A_{N,m} + im\sum_n A_{n,m}(\bar{\omega}\langle V_{N,m} \mid V_{n,m}\rangle - \langle V_{N,m}|\Omega|V_{n,m}\rangle), \tag{45}$$

$$A_{N,m} = \beta_{N,m}^2 C_{N,m} + imP\sum_n C_{n,m}(\bar{\omega}\langle T_{N,m} \mid T_{n,m}\rangle - \langle T_{N,m}|\Omega|T_{n,m}\rangle), \tag{46}$$

where

$$\langle V_{N,m} \mid V_{n,m}\rangle = \int_0^1 V_{N,m}V_{n,m}r\,\mathrm{d}e, \langle V_{N,m}|\Omega|V_{n,m}\rangle = \int_0^1 V_{N,m}\Omega V_{n,m}r\,\mathrm{d}r, \text{ etc.} \tag{47}$$

The coefficients $A_{n,m}$ can be eliminated from equations (45)–(46) resulting in

$$M(\bar{\omega})\cdot C = Ra\cdot C \tag{48}$$

where C is an eigenvector with elements $C_{n,m}$ and the matrix elements $M(\bar{\omega})$ for a given m are

$$M_{Nn} = \sum_l(\beta_{N,m}^2\delta_{Nl} + im\bar{\omega}\langle V_{N,m} \mid V_{l,m}\rangle - im\langle V_{N,m}|\Omega|V_{l,m}\rangle)(\beta_{l,m}^2\delta_{ln} + imP\bar{\omega}\langle T_{l,m} \mid T_{n,m}\rangle - imP\langle T_{l,m}|\Omega|T_{n,m}\rangle). \tag{49}$$

Equation (48) represents an eigenvalue problem which can be solved numerically. The matrix $M(\bar{\omega})$ is shown explicitly as a function of $\bar{\omega}$ because there are actually a pair of eigenvalues, $\bar{\omega}$ and Ra^c, where Ra^c represents the critical Rayleigh numbers, which are solutions of equation (48). Both $\bar{\omega}$ and Ra^c must be real, and for each value of Ra^c there will be a value of $\bar{\omega}$ associated with it. Numerically, we can solve equation (48) by varying $\bar{\omega}$ until the eigenvalues Ra^c become real. The eigenvector C is also obtained from this procedure. By substituting the solutions back into equations (44)–(46), V and T can be calculated.

Before discussing the calculational results, it is useful to describe the roles of the parameters involved. There are three independent variables: K, the dimensionless skin depth; P, the Prandtl number; and the magnetic Taylor number Tm which is a measure of the azimuthal fluid velocity induced by the rotating magnetic field where

$$Tm = \frac{r_0^4 B_0^2 \omega\sigma}{2\rho v^2}. \tag{50}$$

For each set of independent variables the two resultant eigenvalues are Ra^c and $\bar{\omega}$. The size of the matrix M_{Nn}

Table 1
Eigenvalues and critical Rayleigh numbers in a vertical cylinder when no RMF is applied

n	m	β	Ra^c
1	1	2.871	67.96
1	2	4.259	328.9
1	0	4.611	452.0
1	3	5.541	942.5
2	1	6.145	1426
1	4	6.771	2102
2	2	7.571	3286
2	0	7.799	3700

required to accurately calculate the eigenvalues for a given value of m increased as a function of Tm. For $Tm = 10^6$, the largest value of Tm for which the eigenvalues were calculated, a 50×50 matrix was used. This resulted in an upper bound to the error of the eigenvalues of $\pm 0.3\%$.

The zeroth order solution to this problem describes the situation when no rotating magnetic field is applied and $\bar{\omega} = \Omega = 0$. Then, $Ra^c_{n,m} = \beta^4_{n,m}$. The first several lowest values of $\beta_{n,m}$ and $Ra^c_{n,m}$ are listed in Table 1. The values of $Ra^c_{n,m}$ agree with those obtained previously [16].

We now consider the calculational results in the low frequency regime, with $K = 0.1$, and with a Prandtl number appropriate for liquid metals, $P = 0.02$. Figure 5 is a plot of the first few values of Ra^c as a function of Tm. The dashed lines are the value of Ra^c for axisymmetric ($m = 0$) motion and the solid lines are the values of Ra^c for non-axisymmetric ($m \neq 0$) motion. The indices (n, m) are shown for the lowest several modes. As with cylinder rotation [16], the application of an RMF has no influence on the thermoconvective stability of axisymmetric flow modes. But the application of an RMF clearly increases Ra^c for non-axisymmetric modes. Figure 6 is a plot of the eigenvalues $\bar{\omega}$ which correspond to the eigenvalues of Ra^c for non-axisymmetric flow modes shown in Fig. 5. all of the eigenvalues $\bar{\omega}$ depend linearly on Tm for $Tm < 10^3$. Above that value, the eigenvalues of $\bar{\omega}$ for which $n = 1$ diverge from that linear dependence. It is perhaps useful to discuss what $\bar{\omega}$ corresponds to physically. Unlike Ω, $\bar{\omega}$ is not a function of r. Rather, $\bar{\omega}$ is the angular frequency with which the velocity in the z-direction and the temperature profile rotate about the z-axis in the $\bar{\omega}$-direction. for $Tm < 10^3$, $\bar{\omega}$ is of the same order of magnitude as the angular frequency Ω averaged over r.

Figure 7 shows the velocity profiles at the first critical Rayleigh number for several values of Tm. The profiles were calculated with $K = 0.1$ and $P = 0.02$. At the onset of convection, there is an upswelling of warmer fluid on one side of the cylinder and a downswelling of cooler fluid on the other. The normalized velocity in the z-direction as a function of r is shown on the left-hand-side. As Tm increases, the increased azimuthal rotation of the fluid forces V nearer the cylinder wall. On the right-hand-side of fig. 7 is a top-down view of V_{max} and V_{min}, where V_{max} and V_{min} correspond to those positions, as a function of r and $\bar{\omega}$, where V reaches a maximum and minimum value, respectively. As Tm increases, a swirling effect occurs. Both V_{max} and V_{min} occur at smaller values of $\bar{\omega}$ as r decreases. It should also be noted that each of the flow patterns observed rotates about the cylinder with frequency $\bar{\omega}$.

Figure 8 shows the lowest value of Ra^c vs. Tm for four values of K and for $P = 0.02$. For a given value of Tm, Ra^c increases with decreasing K. This trend continues for

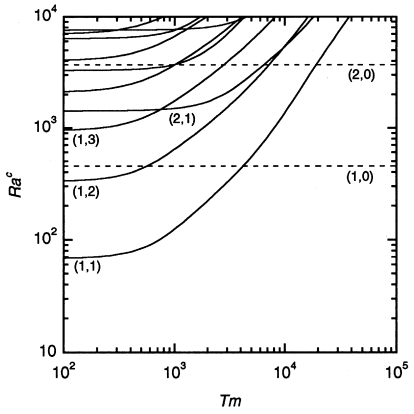

Fig. 5. Critical Rayleigh numbers as a function of magnetic Taylor number. The solid (dashed) lines are for non-axisymmetric (axisymmetric) flow modes. The indices (n, m) are shown for the lowest few modes.

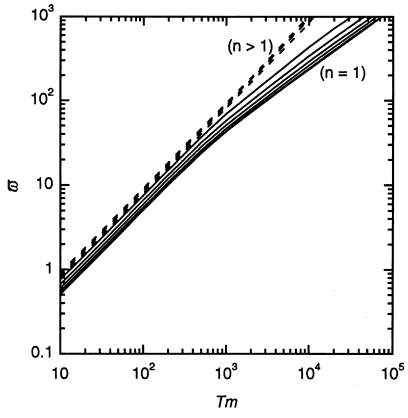

Fig. 6. Rotation frequencies of non-axisymmetric thermoconvective rolls vs. magnetic Taylor number. The values of $\bar{\omega}$ correspond to the first few critical Rayleigh numbers shown in Fig. 5.

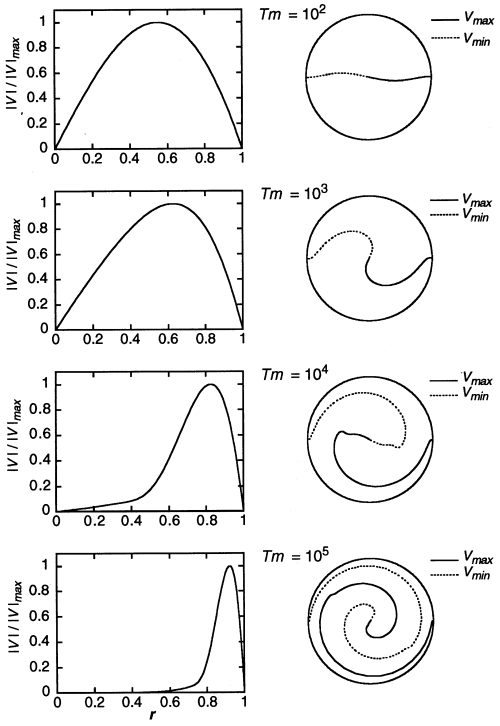

Fig. 7. Velocity profiles in the z-direction at the first critical Rayleigh number for several values of magnetic Taylor number. The left-hand-side shows the normalized velocity as a function of r. The right-hand-side shows the position of the maximum and minimum flow velocity as a function of r and φ. The profiles were calculated with $K = 0.1$ and $P = 0.02$.

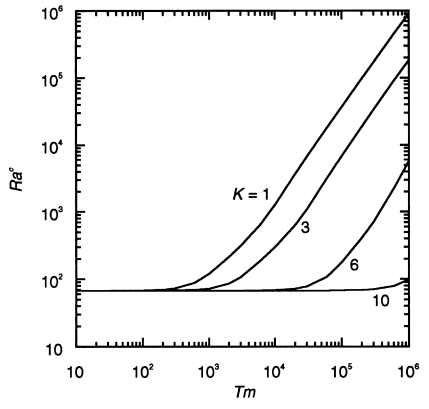

Fig. 8. Critical Rayleigh number vs. magnetic Taylor number for $P = 0.02$ and several values of K.

values of K down to approximately 1. For $K = 1$, the penetration depth of the magnetic field is equal to the cylinder radius and further decreases in K will not increase the average force driving fluid rotation. Therefore, for $K < 1$ the dependence of Ra^c on Tm does not significantly change from that shown for $K = 1$. Figure 9 shows the eigenvalues $\bar{\omega}$ corresponding to the eigenvalues Ra^c shown in Fig. 8. For smaller values of Tm, $\bar{\omega} \propto Tm \propto B_0^2$. The scaling of the roll frequency on the magnetic strength squared is consistent with the theoretical predictions of laminar flow generated by an RMF [4].

The dependence of the onset of instability as a function of Prandtl number is shown in Fig. 10. The data curves were obtained with $K = 0.1$. The figure shows the first critical Rayleigh number, although higher modes may be triggered first for larger Tm. Clearly, an RMF is more

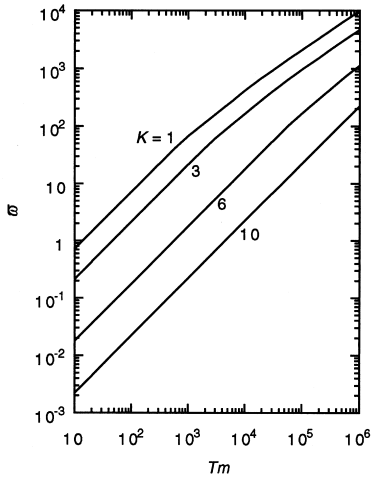

Fig. 9. Rotation frequency vs. magnetic Taylor number for $P = 0.02$ and several values of K.

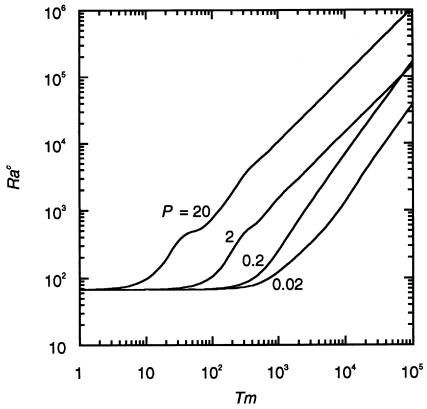

Fig. 10. Critical Rayleigh number vs. magnetic Taylor number for $K = 0.1$ and several values of Prandtl number.

effective at increasing Ra^c for fluids with larger Prandtl numbers. Figure 11 shows the profiles of the maximum velocity and temperature for $K = 0.1$ and $Tm = 10^3$. For $P = 0.02$, the curvature in T_{max} is less than that for V_{max}. This is a result of the relatively high thermal diffusivity of fluids with $P = 0.02$. The profile of T_{max} also tends to stay in close proximity to V_{max}. For $P = 2$, the amount of curvature in V_{max} and T_{max} is roughly equal. A significant angular displacement between V_{max} and T_{max} also exists. The relative curvature and angular displacement between V_{max} and T_{max} both vary as a function of P and Tm. Both V_{max} and T_{max} rotate about the cylinder with rotation frequency $\bar{\omega}$.

5. Discussion

The azimuthal velocity in the preceding sections was calculated based on the assumption that the $\mathbf{v} \times \mathbf{B}$ term could be neglected in comparison to the electric field induced by the external magnetic field. This approximation is valid when [19]

$$\frac{Rm}{\mu_0 \sigma \omega r_0} < 1 \quad \text{for } K \ll 1 \tag{51}$$

$$Rm < 1 \quad \text{for } K \gg 1. \tag{52}$$

Substituting the azimuthal velocity from equations (22) and (23) into these expressions yields

$$\frac{Ha^2}{32} < 1 \quad \text{for } K \ll 1 \tag{53}$$

$$\frac{2Ha^2}{K^2} < 1 \quad \text{for } K \gg 1 \tag{54}$$

where Ha is the Hartmann number defined as

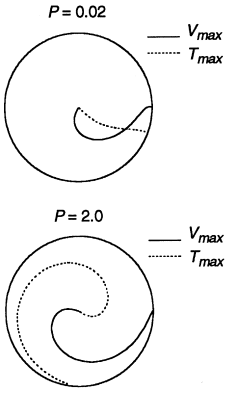

Fig. 11. The position of the maximum temperature and velocity in the z-direction as a function of r and φ. The profiles were calculated with $K = 0.1$ and $Tm = 1000$.

$$Ha = B_0 r_0 \sqrt{\frac{\sigma}{\rho v}}. \tag{55}$$

For typical values $r_0 = 0.01$ m, $\omega = 2\pi \times 60$ s^{-1}, and $v = 3 \times 10^{-7}$ m^2 s^{-1}, we find that the approximations employed are valid when $Tm < O(10^6)$.

The stability analysis assumed a base flow state which is nonzero in the φ-direction. This is correct for the presently considered geometry but is not strictly true as the aspect ratio of the cylinder decreases. For finite cylinders, v_r and v_z are also nonzero, and the ratio of v_r and v_z to v_φ increases as Tm increases. Nevertheless, even for Tm as large as 10^5, the angular velocity of the meridional flow is less than 2% of the base azimuthal flow [7].

The preceding sections have addressed the issue of the Rayleigh instability of fluid driven by an RMF. A second form of instability which can occur is that of Reynolds instability. The rotating fluid will become unstable at some specific magnetic Taylor number, an effect which is similar to that of Taylor instability in a rotating cylinder. The critical value of Tm at which Reynolds instability occurs is a function of the aspect ratio and decreases as the aspect ratio increases [16]. It was found that for an aspect ratio of 1, $Tm^c = 6.2 \times 10^5$, and for an aspect ratio of 6, $Tm^c = 1.3 \times 10^5$. The calculations of Rayleigh instability and fluid flow presented here only have validity when $Tm < Tm^c$.

The laminar flow regime where $Tm < Tm^c$ has been examined recently both by experiments [10] and numerical calculations [7]. Experimentally, temperature fluctuations were measured at Rayleigh numbers above Ra^c as a function of magnetic field strength. The frequency of the fluctuations corresponded to the roll frequency $\bar{\omega}$. It was found that $\bar{\omega} \propto B^2_0$ for magnetic field strengths up to those corresponding to $Tm = 10^4$. Numerically, the dependence of the azimuthal rotation frequency Ω on Tm changed from $\Omega \propto Tm$ to $\Omega \propto Tm^{0.62}$ for $Tm > 10^3$. Although the validity of the calculational results reported here are limited to the laminar regime, it is in this flow regime that the application of an RMF during single crystal growth might prove to be most useful. The occurrence of time-dependent convection can introduce deleterious effects in the grown crystals. In fact, recent crystal growth experiments were done with an RMF strength small enough to avoid time-dependent convection. For example, gallium-doped germanium crystals were grown by the Bridgman method in an RMF with $Tm = 8.5 \times 10^4$ [3] and CdTe was grown from a tellurium solution by the travelling heater method during the Photon 7 microgravity mission with $Tm = 2.8 \times 10^4$ [1]. Thus, the calculational results in the laminar regime are pertinent to understanding stability behavior during crystal growth processes when an RMF is applied, and can serve as a baseline to which further refinements of the theory can be compared.

Acknowledgement

This work was supported by the Microgravity Science and Applications Division of the National Aeronautics and Space Administration.

References

[1] P. Dold, A. Cröll, Th. Kaiser, M. Salk, K.W. Benz, Semiconductor crystals grown under microgravity and in magnetic fields, 33rd Aerospace Sciences Meeting and Exhibit, 1995, AIAA 95-0264.
[2] F.-U. Brückner, K. Schwerdtfeger, Single crystal growth with the Czochralski method involving rotational electromagnetic stirring of the melt, Journal of Crystal Growth 139 (1994) 351–356.
[3] P. Dold, K.W. Benz, Modification of fluid flow and heat transport in vertical Bridgman configurations by rotating magnetic fields, Crystal Research and Technology 32 (1997) 51–60.
[4] P.A. Davidson, J.C. Hunt, Swirling recirculating flow in a liquid-metal column generated by a rotating magnetic field, Journal of Fluid Mechanics 185 (1987) 67–106.
[5] E. Dahlberg, On the action of a rotating magnetic field on a conducting liquid, AB Atomenergi Report AE-447, Sweden, 1972, pp. 1–59.
[6] A.T. Richardson, On the stability of a magnetically driven rotating fluid flow, Journal of Fluid Mechanics 63 (1974) 593–605.
[7] J. Priede, Theoretical study of a flow in an axisymmetric cavity of finite length, driven by a rotating magnetic field, Ph.D. thesis, Latvian Academy of Sciences, Salaspils, Latvia, 1993.
[8] P.A. Davidson, Swirling flow in an axisymmetric cavity of arbitrary profile, driven by a rotating magnetic field, Journal of Fluid Mechanics 245 (1992) 669–699.
[9] T. Robinson, An experimental investigation of a magnetically driven rotating liquid-metal flow, Journal of Fluid Mechanics 60 (1973) 641–664.
[10] M.P. Volz, K. Mazuruk, Flow transitions in a rotating magnetic field, Experiments in Fluids 20 (1996) 454–459.
[11] V.I. Dorinin, V.V. Dremov, A.B. Kapusta, Measurement of the characteristics of the magnetohydrodynamic flow of mercury in a closed cylindrical vessel, Magnetohydrodynamics 3 (1973) 138–140.
[12] P. Dold, K.W. Benz, Convective temperature fluctuations in liquid gallium in dependence on static and rotating magnetic fields, Crystal Research and Technology 30 (1995) 1135–1145.
[13] Y.M. Gelfgat, L.A. Gorbunov, V. Kolevzon, Liquid metal flow in a finite length cylinder with a rotating magnetic field, Experiments in Fluids 15 (1993) 411–416.
[14] J.C. Buell, I. Catton, Effect of rotation on the stability of a bounded cylinder layer of fluid heated from below, Physics of Fluids 26 (1983) 892–896.
[15] G.S. Charlson, R.L. Sani, On thermoconvective instability in a bounded cylindrical fluid layer, International Journal of Heat and Mass Transfer 14 (1971) 2157–2160.
[16] C.S. Yih, Thermal instability of viscous fluids, Quarterly of Applied Mathematics 17 (1959) 25–42.
[17] R.U. Barz, G. Gerbeth, U. Wunderwald, E. Buhrig, Y.M. Gelfgat, Modelling of the isothermal melt flow due to rotating magnetic fields in crystal growth, Journal of Crystal Growth 180 (1997) 410–421.
[18] M.R.E. Proctor, Instability of stratified fluid in a vertical cylinder, in: G.K. Batchelor, J.M. Nitsche, (Eds.), Journal of Fluid Mechanics 252 (1993) 419–448.
[19] R. Moreau, Magnetohydrodynamics, Kluwer Academic, Dordrecht, 1990, pp. 32–38.